AGU PUBLICATIONS

JGR

Journal of Geophysical Research: Atmospheres

RESEARCH ARTICLE
10.1002/2017JD027516

Key Points:
- RapidScat and CCMP data sets agree on much of the seasonal variability of ocean vector winds near the Philippines
- RapidScat and CCMP agree on many aspects of the diurnal variability of winds near the Philippines
- Daytime onshore and nocturnal offshore flow patterns affect the diurnal cycle of winds up to ~200 km west of Luzon, Philippines

Supporting Information:
- Supporting Information S1

Correspondence to:
T. J. Lang,
timothy.j.lang@nasa.gov

Citation:
Lang, T. J. (2017). Investigating the seasonal and diurnal cycles of ocean vector winds near the Philippines using RapidScat and CCMP. *Journal of Geophysical Research: Atmospheres*, *122*, 9668–9684, https://doi.org/10.1002/2017JD027516

Received 26 JUL 2017
Accepted 7 SEP 2017
Accepted article online 10 SEP 2017
Published online 27 SEP 2017

Investigating the Seasonal and Diurnal Cycles of Ocean Vector Winds Near the Philippines Using RapidScat and CCMP

Timothy J. Lang[1]

[1]National Aeronautics and Space Administration George C. Marshall Space Flight Center, Huntsville, AL, USA

Abstract The seasonal and diurnal cycles of ocean vector winds in the domain of the South China Sea are characterized and compared using RapidScat and the Cross-Calibrated Multi-Platform (CCMP) data sets. Broad agreement in seasonal flow patterns exists between these data sets during the year 2015. Both observe the dramatic reversal from wintertime trade winds (November–April) to westerly flow associated with the summer monsoon (May–October). These seasonal changes have strong but not equivalent effects on mean wind divergence patterns in both data sets. Specifically near the Philippines, the data sets agree on several aspects of the seasonal mean and diurnal cycle of near-surface vector winds and divergence. In particular, RapidScat and CCMP agree that daytime onshore and nocturnal offshore flow patterns affect the diurnal cycle of winds up to ~200 km west of Luzon, Philippines. Observed disagreements over the diurnal cycle are explainable by measurement uncertainty, as well as shortcomings in both data sets.

Plain Language Summary It is important to know how satellite-based wind data sets compare with one another, in order to understand basic wind patterns in the South China Sea—an area that is strategically important to many countries. The seasonal and daily variability of low-altitude winds over the South China Sea was studied using two independent satellite data sets that report both wind speed and direction. One of these data sets spans a few decades, while the other is much shorter but more precisely measures the daily cycle of winds. The two data sets agree well on seasonal wind shifts during the year 2015. Both observe the dramatic reversal from winter trade winds (November–April) to the summer monsoon (May–October). Both data sets also agree on wind shifts throughout a typical day near the island of Luzon in the northern Philippines. Relative to the average wind pattern, in the morning winds blow onshore, while overnight they reverse and blow offshore as far as 200 km from the coast. The results give us confidence that we can use both data sets to understand different parts of the wind climatology near the Philippines.

1. Introduction

The South China Sea is a region of great meteorological variability and is strategically significant from the political (e.g., Hayton, 2015), economic (e.g., Zheng et al., 2013, 2012), and military (e.g., United States Department of Defense, 2015) perspectives. Because of this, there is substantial interest in improving subseasonal to seasonal weather forecasting in this region (Chan et al., 1998; Chen et al., 2015; Fukutomi & Yasunari, 2002; Lau et al., 2000; Wu & Zhang, 1998; Yang et al., 2015), as well as documenting interannual variability (e.g., Fang et al., 2006).

This region is broadly affected by the East Asian monsoon, which causes seasonal reversals of winds in and around the South China Sea (Chen & Chen, 1995; Ciesielski & Johnson, 2006; Hasager et al., 2016; Wang et al., 2004). Specifically, easterly trade winds during the boreal winter months are replaced by monsoon westerlies during boreal summer. Beyond this seasonal variability, winds and precipitation in this region are impacted intraseasonally by the eastward propagating 40–50 day Madden Julian Oscillation (MJO) (Zhang, 2005). During the boreal summer, a form of the MJO—called the Boreal Summer Intraseasonal Oscillation (BSISO)—can occur, and it is distinguished by both northward and eastward propagation of fluctuations in (among other atmospheric state parameters) winds and precipitation (Fu & Wang, 2004; Lee et al., 2013).

The MJO and BSISO have complex interactions with the South China Sea and Maritime Continent region, which includes the islands encompassing the countries of the Philippines, Indonesia, and others. Indeed, the Maritime Continent often interacts significantly with the propagation of the MJO signal (Birch et al., 2016;

Vitart and Molteni, 2010). This effect may be linked to the strong diurnal cycles of winds and precipitation observed in this region (Huang et al., 2010; Ichikawa & Yasunari, 2006; Li et al., 2010; Love et al., 2011; Ploshay & Lau, 2010). Therefore, it has been hypothesized that further improvements to subseasonal and seasonal forecasting in and around the South China Sea region will require improved understanding of the complex interplay between intraseasonal oscillations such as the MJO and BSISO and the island-driven diurnal cycles (Ho et al., 2008; Kim et al., 2016).

Key to any forecasting improvements is gaining a better understanding of the physical processes controlling meteorological variability in this region. This requires analysis of a large variety of data sets and is the focus of an upcoming field campaign called Propagation of Intraseasonal Tropical Oscillations (Propagation of Intraseasonal Tropical Oscillations, 2017). Propagation of Intraseasonal Tropical Oscillations (PISTON) is planned to be focused on the western coastal region of the island of Luzon in the Philippines. One of the reasons is that this area is strongly impacted by island-driven diurnal cycle effects, making it a natural laboratory for understanding how intraseasonal and diurnal atmospheric and oceanic oscillations interact.

Before addressing intraseasonal variability, however, the fundamental seasonal and diurnal variability of winds is this region needs to be better understood. The hypothesis of this study is that these diurnal and seasonal changes are very large and thus could mask potentially more subtle intraseasonal changes, if the intraseasonal analysis did not properly account for them. Thus, the focus of the present study is on quantifying the seasonal and diurnal cycles of near-surface winds in the vicinity of the Philippines, and a follow-on study will address the intraseasonal variability.

Ocean vector winds have been provided routinely by satellite for multiple decades (Hilburn et al., 2016; Sharma & D'Sa, 2008; Zierden et al., 2000); however, most of these satellites have been in Sun-synchronous orbits and thus pass over the same region at fixed times of the day. A model-enhanced data set, called Cross-Calibrated Multi-Platform (CCMP) (Atlas et al., 2011; Wentz et al., 2015), has sought to overcome this limitation by assimilating observations from multiple satellites, as well as surface-based observations. CCMP covers multiple decades (1987–2016 as of this study) and is 6-hourly resolution—the minimum needed to resolve (at least coarsely) a diurnal wind feature.

There is interest in determining whether CCMP can quantitatively characterize key aspects of the diurnal winds near the Philippines, particularly given the inherent uncertainties associated with the realism of this model-enhanced data set (McGregor et al., 2017). Recently, a scatterometer instrument called RapidScat (Lin et al., 2017; Madsen & Long, 2016; Paget et al., 2016; Wang et al., 2017) operated for nearly 2 years on the International Space Station (ISS). Since the ISS is in a non-Sun-synchronous orbit, RapidScat provided observations in the same location throughout the diurnal cycle. This provides an independent data set to compare against CCMP. RapidScat can be used to study the diurnal cycle of winds at higher temporal resolution than CCMP, but improved understanding of its ability to quantify the diurnal cycle is needed. There is also interest in examining the diurnal cycle of near-surface wind divergence, since this parameter is rarely examined in detail in this region. For example, Wood et al. (2009) examined the diurnal cycle of near-surface wind divergence but focused on global-scale observations, while Tang et al. (2014) only focused on the global diurnal cycles of zonal and meridional winds without considering divergence. Meanwhile, the modeling work of Park et al. (2011) indicated important diurnal variability in divergence near the Philippines.

The goals of this study are to (1) determine diurnal cycle of ocean winds near the Philippines (especially west of the island of Luzon) at high spatial/temporal resolution (0.25° and 2 hourly); (2) examine how well CCMP characterizes the wind climatology and diurnal cycle relative to RapidScat; and (3) determine near-surface divergence fields near the Philippines along with their diurnal cycles. Achieving these goals will serve as an important first step toward improving our understanding of the seasonal and diurnal variability of winds near the Philippines, thereby setting the stage for future investigation into intraseasonal variability, particularly using the long-term CCMP data set as well as field observations from PISTON.

2. Data and Methodology

2.1. RapidScat

RapidScat was a Ku band scatterometer that operated on the ISS from October 2014 to August 2016 (RapidScat Project, 2016). This instrument was very similar to the QuikSCAT instrument, as it was built from

QuikSCAT spare parts, and therefore the data have been processed very similarly to the QuikSCAT data set (Fore et al., 2013). The data set that was used in this study was the v1.0 Level 2B climate-quality ocean wind vectors at 12.5 km resolution. This data set is processed using the full antenna footprints without any range subdivisions, and also features calibration corrections for the low signal-to-noise ratio (SNR) episodes that periodically affected the instrument (RapidScat Project, 2016). According to Havens and Poulson (2016), RapidScat had 92.5% uptime, with most outages caused by visiting vehicles to the ISS. In addition, approximately 80% of the data were identified as good quality, with reduced-quality observations commonly caused by ISS altitude and attitude variability. RapidScat is able to measure the individual zonal wind (U) and meridional wind (V) components with better than 0.7 m s^{-1} precision relative to other scatterometers (Wang et al., 2017).

The entire period of RapidScat observations (October/2014 to August/2016) was analyzed in this study. Each orbit granule was analyzed for possible intersection with the analysis domain of 5°S to 20°N and 110–130°E (see Figure 1 for a depiction of the analysis domain). For each granule that was, divergence was calculated in swath coordinates using a centered, second-order, finite-difference approach (i.e., Derivatives First, Averages Second or DFAS in the nomenclature of O'Neill et al., 2015), and all valid U, V, and divergence observations from each wind vector cell (WVC) inside the domain were saved (along with geolocation and timing information).

Afterward, these data were assigned to a 0.25° resolution grid for the domain using a nearest neighbor approach. Data also were assigned to 2 h bins during the diurnal cycle, again using a nearest neighbor approach. Finally, subsetting by month and year was done. Analysis gridpoints with fewer than 400 RapidScat observations during the entire 22 month data set were not considered in this study. This eliminated many coastal gridpoints with measurements of dubious quality due to the presence of land.

Sensitivity studies using different averaging techniques or more aggressive filtering on data quality flags were also performed. Under certain circumstances (e.g., polar-orbiting satellites), the binning-and-averaging technique described above is known to cause biases in satellite mean fields on monthly and longer time scales (Patoux & Levy, 2013). In order to gauge the impact of any possible biases resulting from binning and averaging, a sensitivity study was performed where the RapidScat data set was first interpolated to daily grids using the technique of Zeng and Levy (1995). In order to mitigate biases, this technique uses a custom data weighting that works in both distance and time (their equation (2)), and for this sensitivity study the characteristic distance and time scales were set to 100 km and 1 day, respectively. The daily grids were then accumulated into seasonal means. Note that this interpolation technique precludes examining diurnal evolution, and thus was used only for studying differences in seasonal means. A sensitivity study also was performed using standard binning and averaging but excluding all wind vector cells (WVCs) containing positive rain flags. These sensitivity study results will be presented in section 3.

2.2. Cross-Calibrated Multi-Platform

This study also analyzed the Version 2.0, Level 3.0 CCMP ocean vector wind data set (Wentz et al., 2015). This data set is available for 1987–2016 (as of this study) at 0.25° spatial resolution and 6 h temporal resolution. This data set is composed of model-assimilated satellite and buoy measurements of ocean winds. The period of time analyzed in this study was 3 October 2014 through 30 May 2016, which comprises the entire sampling overlap between RapidScat and CCMP (as of the time of this study; CCMP is planned to be extended into the future). During this time, satellite ocean wind platforms included Advanced Scatterometer on MetOp-A (ASCAT-A), WindSat, Global Precipitation Measurement (GPM) Microwave Imager (GMI), Advanced Microwave Scanning Radiometer 2 (AMSR-2), and the Special Sensor Microwave Imager/Sounder (SSMI/S) on the F17 satellite. Many of these satellites only observe at fixed times of the day, although GMI varies throughout the diurnal cycle similar to RapidScat (Hou et al., 2014). However, GMI only observes wind speeds, not vectors. Crucially, CCMP does not include RapidScat; therefore, it constitutes an independent data set, which simplifies comparative analysis.

CCMP data also were subsetted to the same spatial domain as RapidScat. However, CCMP already was prebinned at 6 h resolution, so no further temporal binning was performed. Divergence was calculated on the spatial grid using a centered, second-order, finite-difference approach with no additional smoothing. Subsetting of CCMP data by month also was done.

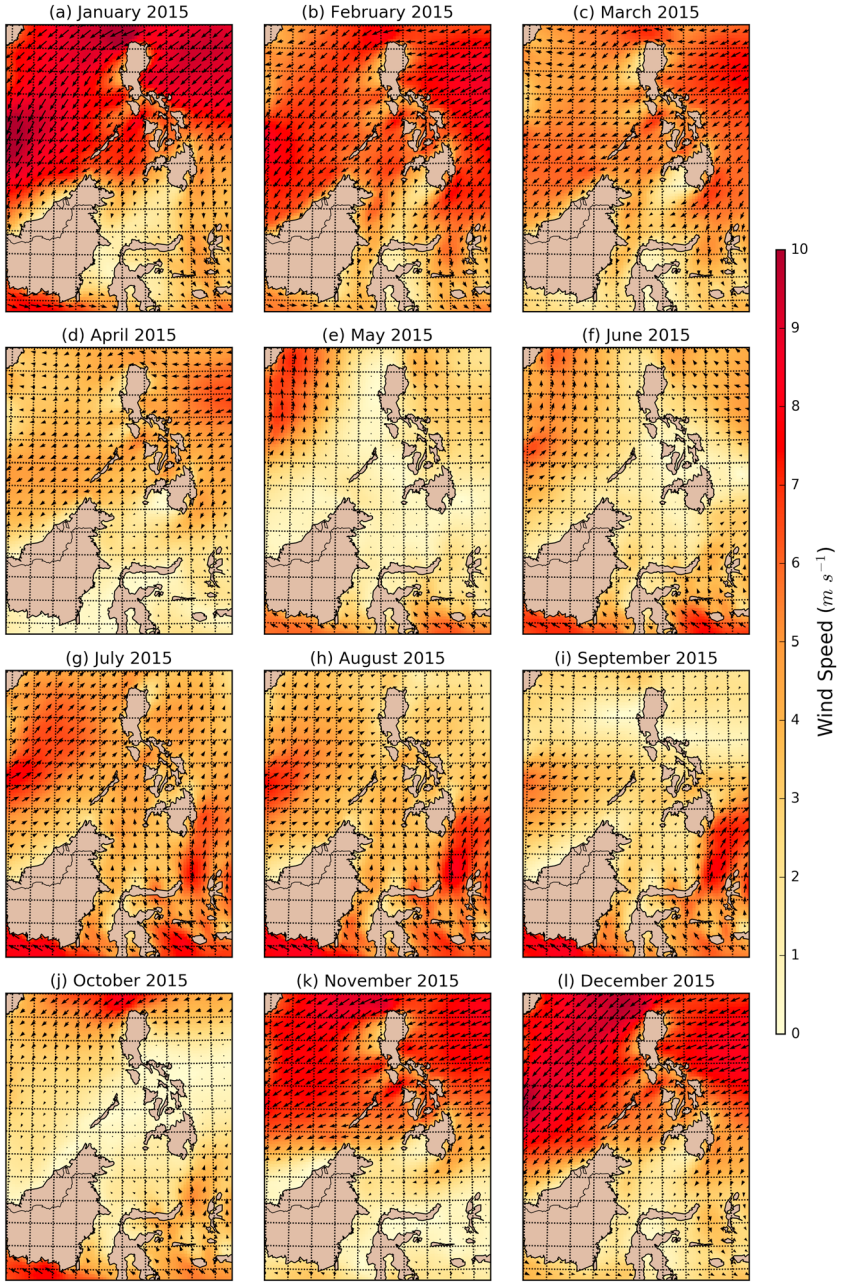

Figure 1. CCMP monthly mean winds for the year 2015, for the domain of interest. Wind speeds are indicated by the colors, while vectors indicate direction and relative magnitude. Gridlines are every 2°. Vectors have been thinned by a factor of 4.

3. Results

3.1. CCMP Monthly Mean Flow

In order to understand the comparisons between CCMP and RapidScat, they must be viewed in context of the typical wind climatology for this region. Figure 1 shows monthly mean winds, derived from analysis of all 2015 CCMP data, for the region near the Philippines, including portions of the South China Sea and Philippine Sea. What is observed is easterly to northeasterly trade winds in January (Figure 1a), which then begin to reverse during the premonsoon spring, ultimately leading to strong southwesterly flow during the peak monsoon months of July–August (Figures 1g and 1h) (e.g., Xie et al., 2007). This pattern weakens in the fall, and then during November and December (Figures 1k and 1l) the trade winds reestablish themselves.

During wintertime (Figures 1a, 1b, and 1l), the trade wind strength is clearly reduced in the wake of the Philippine archipelago—notably the islands of (from north to south) Luzon, Mindoro, and Mindanao. (For a political map of the Philippines including island names, see National Geographic Society, 2014.) In addition, there is cyclonic curvature of the winds off the northwest coast of Luzon. This curvature also was observed by Wang et al. (2008) using QuikSCAT. Between major islands in the archipelago there are indications of intensified gap flows, such as between Luzon and Mindoro, as well as between Mindoro and Panay (Gierach et al., 2012). This basic trade wind pattern—with wake stagnation, cyclonic curvature, and gap flows—still dominates in March and April (Figures 1c and 1d), but wind speeds are reduced.

In May (Figure 1e), however, there is a dramatic weakening of the winds west of the Philippines. As the southwesterly monsoon flow sets up in summer of the west coast (Figures 1f–1h), there even are indications of wake stagnation to the northeast of Luzon, especially in July (Figure 1g). However, mean strength of the monsoon flow never reaches the wintertime trade wind strength, so there is much less cyclonic curvature and weaker gap flows near the Philippines themselves. There is a very interesting reversing gap flow between the Indonesian islands of Sulawesi and Halmahera, which is strongest in the southerly direction during July–September (Figures 1g–1i) and in the northerly direction during January–March (Figures 1a–1c). (For a political map of Indonesia including island names, see National Geographic Society, 2014.) During October (Figure 1j), calm winds return to the central Philippines, while weak trades begin to set up north of Luzon, leading to some cyclonic curvature northwest of the island.

Based on the climatology in Figure 1, the six months during 2015 with the strongest trade wind signatures (northeasterly flow with wake stagnation, cyclonic curvature, and gap flows) west of the Philippines are January–April (Figures 1a–1d) and then November–December (Figures 1k and 1l). For simplicity, this period will be called November–April. The other six months, May–October (Figures 1e–1j), feature primarily calm to southwesterly flow west of the archipelago, with only the transition month of October featuring any significant trade wind activity nearby. Even then, this occurs only in the northern Philippines. Therefore, November–April and May–October will be examined separately going forward.

3.2. Seasonal Comparison—CCMP Versus RapidScat

First, CCMP will be compared with RapidScat on a seasonal mean basis (i.e., monsoon or May–October, and nonmonsoon or November–April). Since RapidScat started data collection in late 2014, and ended its data collection before its second year completed, the primary focus for seasonal comparisons will be on CCMP and RapidScat during 2015 only. Figure 2 shows the mean flow during May–October 2015 with RapidScat (Figure 2a) and CCMP (Figure 2b), while the November–April 2015 results for both are shown in Figures 2c and 2d, respectively. Grid points with less than 400 total samples during the entire 22 month data set were excluded from the corresponding RapidScat map, masking most data near coastlines (though conspicuously not near the west coast of Luzon).

For May–October 2015, the two data sets provide very similar results, with three notable differences: (1) CCMP provides more complete spatial coverage; (2) certain regions show notable differences in wind speed between RapidScat and CCMP; and (3) RapidScat shows cyclonic curvature of winds, ostensibly due to blocking effects, within the Gulf of Tomini (Sulawesi), while CCMP does not have this feature. Both data sets indicate a small gap flow due to terrain near the city of Gorontalo on north Sulawesi.

For November–April 2015, again results are very similar between the two data sets, and again CCMP provides more complete spatial coverage while notable wind speed differences preferentially occur in certain regions. Due to mean wind direction, there are no distinct differences within the Gulf of Tomini; however, there is an indication of northerly gap flow west of the island of Pulau Taliabu that is seen by RapidScat, which CCMP does not resolve. Near the Philippines, RapidScat appears to indicate greater wake stagnation downwind of Panay and Negros islands, and stronger gap flows between most western islands in the archipelago. However, on the windward side of the Philippines, CCMP has more information closer to the coastlines, and this appears to indicate slowing of the trade winds as they encounter larger islands, such as Luzon and Mindanao. RapidScat does not resolve these features, in part because coastal data are limited within the Philippine archipelago.

Figure 3 integrates the seasonal comparisons over the entire domain. Because CCMP wind vectors are provided as individual wind components (U and V), these components are compared separately. Over the

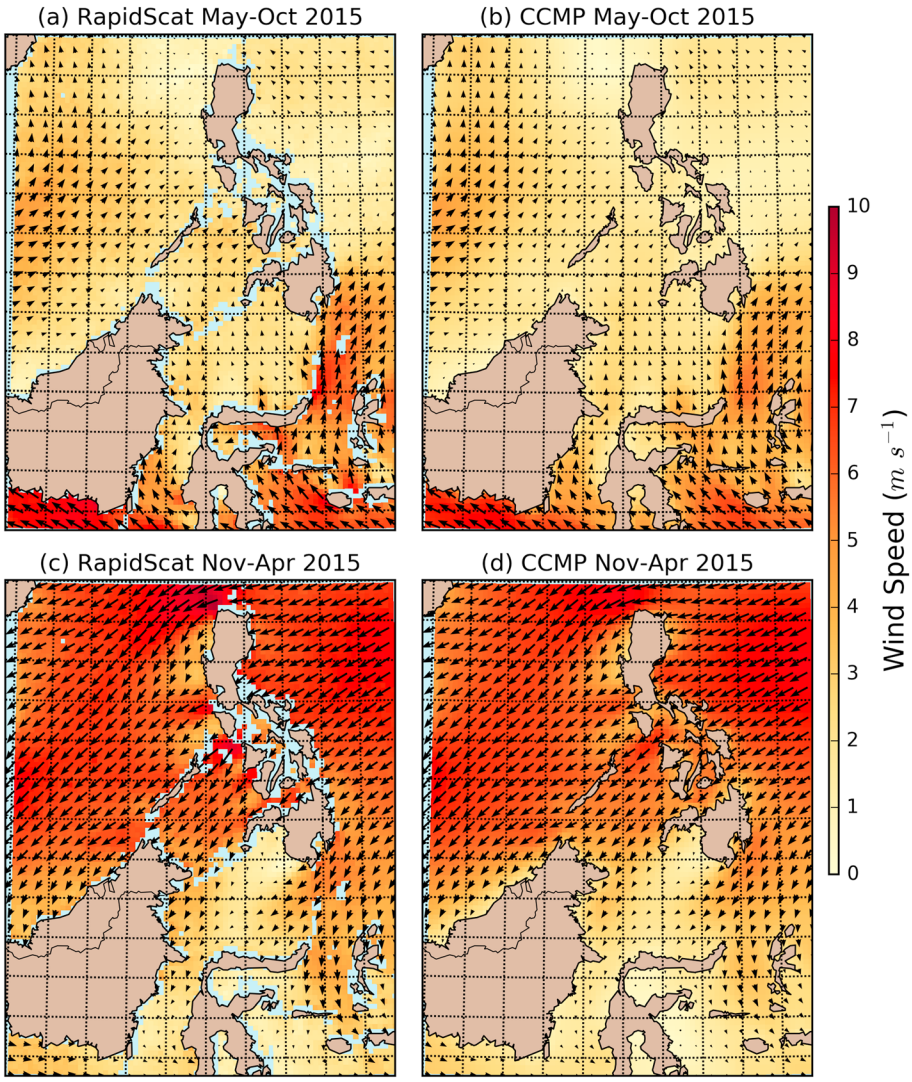

Figure 2. Seasonal mean winds from RapidScat and CCMP using the bin-and-average technique. Wind speeds are indicated by the colors, while vectors indicate direction and relative magnitude. Gridlines are every 2°. Vectors have been thinned by a factor of 3. (a) RapidScat May–October 2015. (b) CCMP May–October 2015. (c) RapidScat November–April 2015. (d) CCMP November–April 2015.

entire domain, no significant overall offset is seen between the two data sets in either *U* or *V*, and standard deviations are only ~0.2 m s^{-1}. Although some outliers are indicated in the Figure 3 histograms, as well as the previously described differences in Figure 2, there is overall very good agreement between the two independent data sets for this domain, regardless of season.

The Zeng and Levy (1995) interpolation approach also was used to produce RapidScat seasonal means, with the results shown in Figure S1 in the supporting information. Overall, the seasonal patterns are very similar to the bin-and-average approach, with many of the same similarities and differences between RapidScat and CCMP. The one big change, however, is that Zeng and Levy (1995) enables estimates in poorly sampled coastal regions, due to the 100 km characteristic distance interpolation. Using the 400-sample threshold leads to slightly worse agreement between RapidScat and CCMP in the domain average (Figure S2), but individual component mean offsets and standard deviations remain <0.5 m s^{-1}. If the 400-sample threshold is removed, agreement worsens considerably (not shown); though the more sophisticated interpolation provides more aesthetically pleasing results, the filled-in RapidScat data near coastlines still should not be trusted.

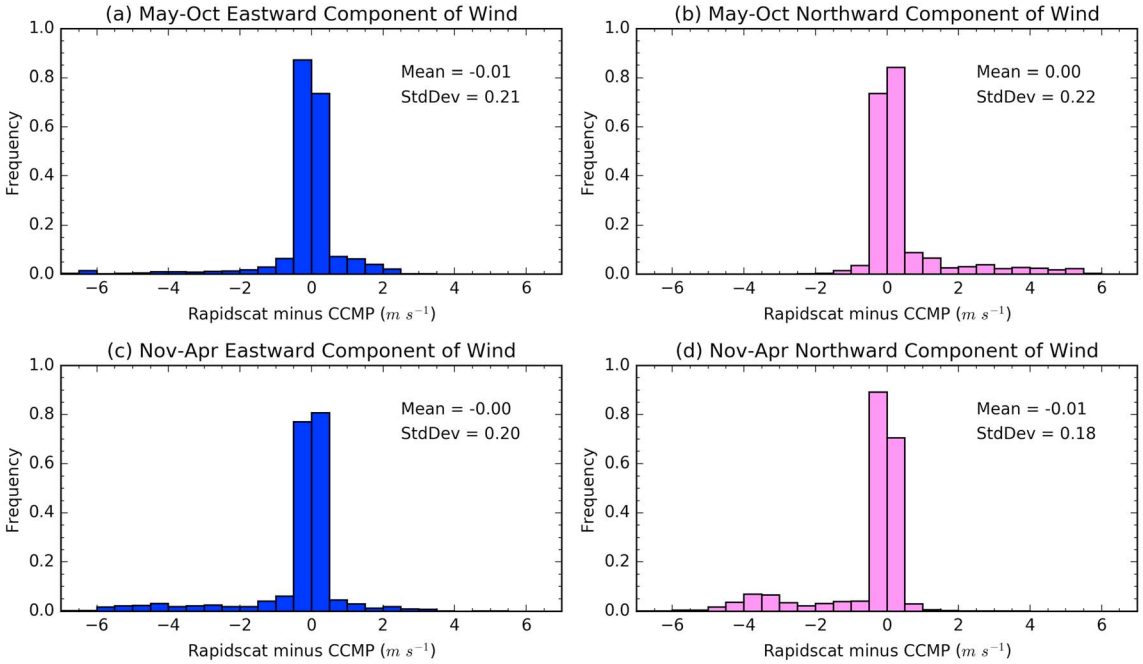

Figure 3. Whole-domain normalized histograms of RapidScat minus CCMP wind components for the 2015 seasonal averages. Also indicated are the mean and standard deviation of these differences. (a) May–October 2015, eastward component (*U*). (b) May–October 2015, northward component (*V*). (c) November–April 2015, eastward component (*U*). (d) November–April 2015, northward component (*V*).

The bin-and-average approach, but with rain flags removed, leads to seasonal results that are very similar to just keeping the rain-flagged data (Figures S3 and S4). However, removing the rain-flagged data eliminates 12.4% of the overall data set, so the 400-sample threshold becomes more stringent and reduces further the data coverage near coastlines/islands.

Overall, based on the sensitivity studies, it is concluded that all of the above methods are defensible approaches to interpolating the RapidScat data set for seasonal comparisons to CCMP, for this domain. None appear to introduce very large biases or variability in excess of 0.5 m s^{-1} in the domain mean, relative to CCMP. In addition, the RapidScat methodologies all provide similar results in areas that are notably different than CCMP (e.g., the cyclonic curvature over the Gulf of Tomini). Since the bin-and-average approach provides the most flexibility for examining diurnal wind behavior, this interpolation approach will be the focus during the next section.

3.3. Diurnal Wind Comparison—CCMP Versus RapidScat

Since CCMP provides 6 h resolution, and RapidScat samples throughout the day, the diurnal cycles of winds in both data sets were compared. For CCMP this was straightforward—simply average the winds at each 6 h time step over each 6 month time period, then subtract the average wind at that time step from the mean seasonal flow. For RapidScat the data were binned with 2 h time steps, and then each grid point was fitted via least squares analysis to a diurnal harmonic following Gille et al. (2005, 2016). The analysis was done for the entire temporal overlap between RapidScat and CCMP (roughly October 2014 through May 2016; Section 2.2). The diurnal harmonic at each time was then subtracted from the mean.

Results are shown in Figure 4. For ease of comparison, only the RapidScat results at 0, 6, 12, and 18 UTC are shown. At 0 UTC RapidScat (Figure 4a) indicates anomalously strong southeasterly offshore flow (relative to the overall mean) northwest of Luzon. Manila (which is on Luzon) is 8 h ahead of UTC, so this is around 8 a.m. Local time. CCMP also indicates similar anomaly winds northwest of Luzon (Figure 4e), but magnitudes are reduced.

Moving to 6 UTC (Figure 4b), or 14 Local in Luzon, anomalous onshore flow is now seen west of Luzon, a pattern also seen in CCMP at this time (Figure 4f). However, at this time only, the Philippines onshore pattern

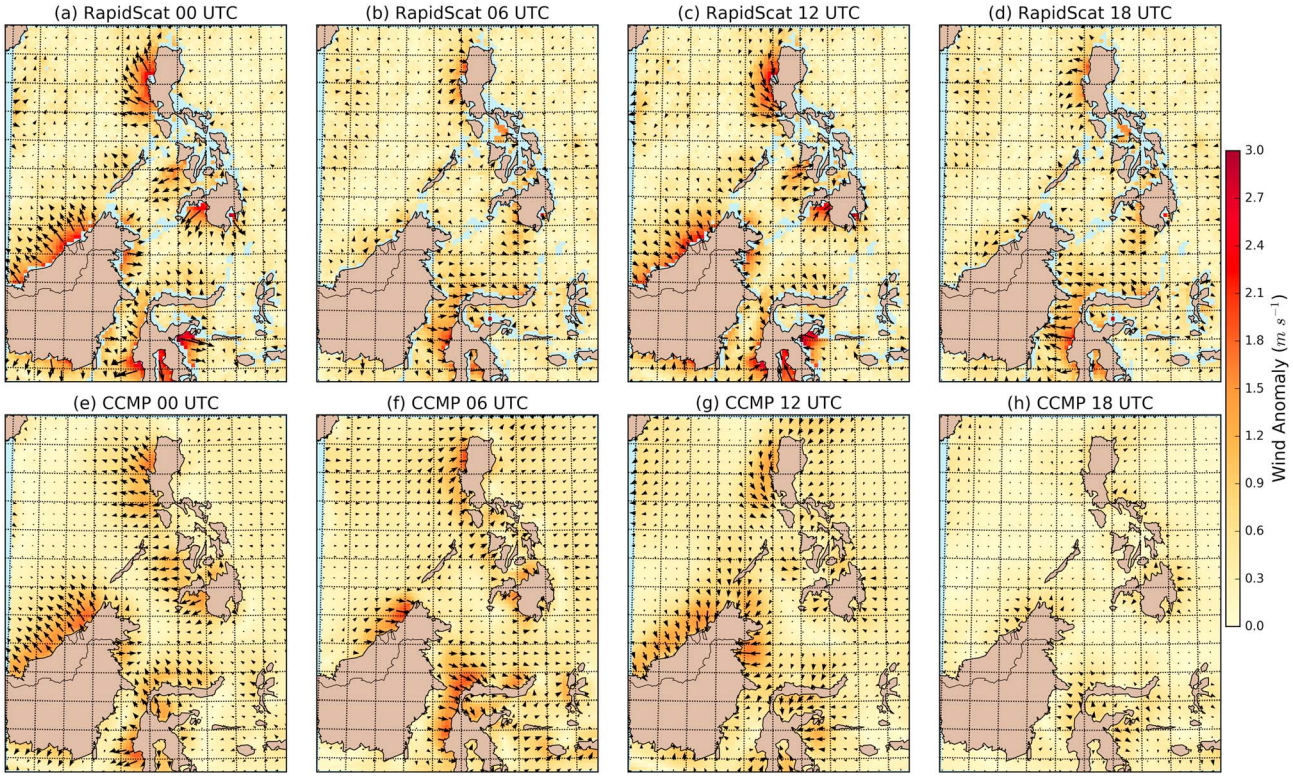

Figure 4. Anomaly winds relative to the 3 October 2014 through 30 May 2016 RapidScat diurnal harmonic mean and CCMP mean, broken down by 6 h portions of the diurnal cycle. Wind speed anomalies are indicated by the colors, while vectors indicate direction and relative magnitude of the wind anomalies. Gridlines are every 2°. Vectors have been thinned by a factor of 3. (a) RapidScat at 0 UTC. (b) RapidScat at 6 UTC. (c) RapidScat at 12 UTC. (d) RapidScat at 18 UTC. (e) CCMP at 0 UTC. (f) CCMP at 6 UTC. (g) CCMP at 12 UTC. (h) CCMP at 18 UTC.

is stronger in the CCMP data set. Broadly onshore wind patterns are also observed in both data sets northwest of Sulawesi and around the northern tip of Borneo, and these flows are stronger in CCMP as well. At 12 UTC (20 local; Figures 4c and 4g), both data sets suggest northerly flow anomalies west of Luzon, but RapidScat's anomalies are stronger. Onshore flow also continues near Borneo and Sulawesi, though RapidScat's pattern is more spatially variable. Finally, at 18 UTC (2 Local; Figures 4d and 4h), RapidScat suggests much stronger easterly offshore flow west of Luzon, though CCMP has the same directionality. Though the temporal analyses are different, the results for both data sets are qualitatively similar to the simulated diurnal cycles for this region as characterized by Ploshay and Lau (2010) and Wang et al. (2013). Though not shown here, the results for the entire RapidScat data set, through August 2016, were very similar to the truncated data set that matched CCMP's temporal coverage. This suggests that future analyses with more complete CCMP coverage of 2016 would not produce significantly different results.

Since RapidScat lasted less than 2 years, it is important to ensure that the diurnal sampling was relatively uniform in most regions. This would improve confidence in the results presented in Figure 4. Toward that end, Figure S5 shows the standard error of RapidScat winds (averaging the results for the separate *U* and *V* components) as a function of time of day, with areas of less than 400 samples thresholded. The standard error is <0.5 m s^{-1} over much of the domain, throughout the day, with the main exceptions being near coastlines and islands. In the domain mean, the standard error is roughly constant throughout the day (~0.3 m s^{-1}). In addition, near the west coast of Luzon the coastal sampling artifacts are limited, and standard errors are well behaved throughout the day.

Figure 5 integrates the diurnal cycle comparisons shown in Figure 4, by presenting histograms of anomaly wind differences between RapidScat and CCMP. The domain of interest has been shrunk to focus only near the west coast of Luzon (see Figure 6 for a representation of this domain). The mean offsets support the qualitative inferences from Figure 4. Moreover, all offsets are within ±0.4 m s^{-1} for each wind component, and

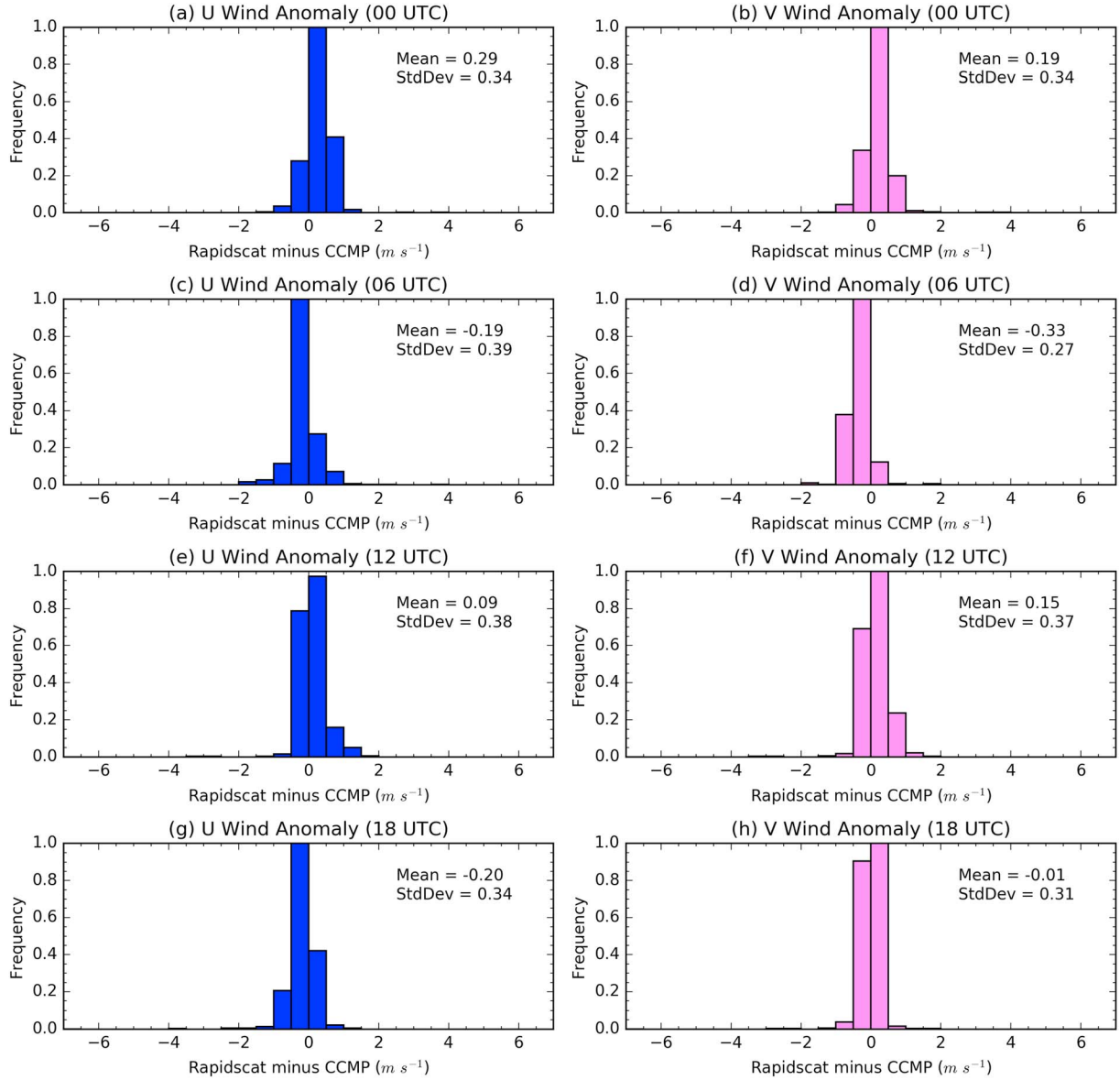

Figure 5. Normalized histograms of anomaly wind differences, relative to the 3 October 2014 through 30 May 2016 RapidScat diurnal harmonic mean and CCMP mean, broken down by 6 h portions of the diurnal cycle. Also indicated are the mean and standard deviation of these differences. Domain of consideration is same as the one shown in Figure 7. (a) *U* anomaly, 0 UTC. (b) *V* anomaly, 0 UTC. (c) *U* anomaly, 6 UTC. (d) *V* anomaly, 6 UTC. (e) *U* anomaly, 12 UTC. (f) *V* anomaly, 12 UTC. (g) *U* anomaly, 18 UTC. (h) *V* anomaly, 18 UTC.

the standard deviations of these offsets are all less than 0.4 m s^{-1}. These differences are only slightly higher than standard errors associated with the RapidScat diurnal sampling shown in Figure S5. Very similar differences are seen even if the entire domain in Figure 4 is analyzed (not shown). Overall, the results suggest that the diurnal wind differences are within the measurement uncertainties for both RapidScat and CCMP (Atlas et al., 2011; Lin et al., 2017; Wang et al., 2017).

In order to better understand the high-resolution variability of winds near the rainfall maximum west of Luzon (Park et al., 2011; Xie et al., 2006), the diurnal harmonic of RapidScat winds near Luzon was broken out at 2 h resolution (Figure 6). The entire RapidScat data set was used for this analysis. The goodness of fit (i.e., square of the correlation coefficient, or R^2) parameter was also calculated, and the $R^2 = 0.5$ contour is also shown in Figure 6. Since both the eastward and northward components of the wind (i.e., *U* and *V*) were fit separately, the average of these two R^2 values is what is shown (as might be expected from the coastline

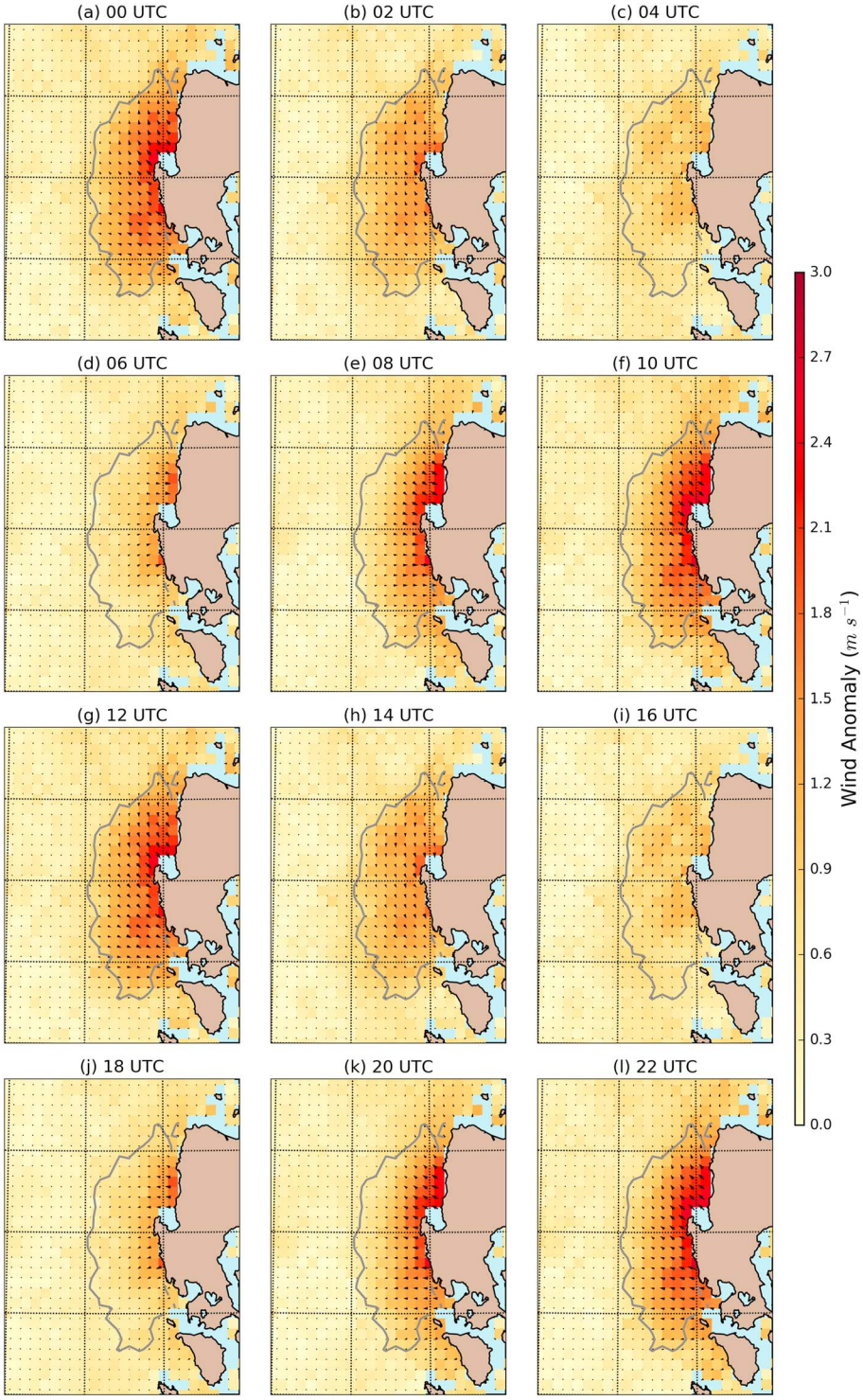

Figure 6. Anomaly wind harmonics relative to the average for the entire RapidScat data set, broken down by 2 h portions of the diurnal cycle. Wind speed anomalies are indicated by the colors, while vectors indicate direction and relative magnitude of the wind anomalies. Gray contour indicates $R^2 = 0.5$. Gridlines are every 2°. Vectors have not been thinned.

shape and Figures 3 and 4, the fit to *U* is significantly better than to *V*). A clear pattern of alternating onshore and offshore flow near Luzon emerges from this figure, where the diurnal harmonic R^2 is greater than 0.5. Offshore flow is strongest at 22 and 0 UTC (Figures 6a and 6l; morning Local), while onshore flow is strongest at 10 and 12 UTC (Figures 6f and 6g; early evening Local).

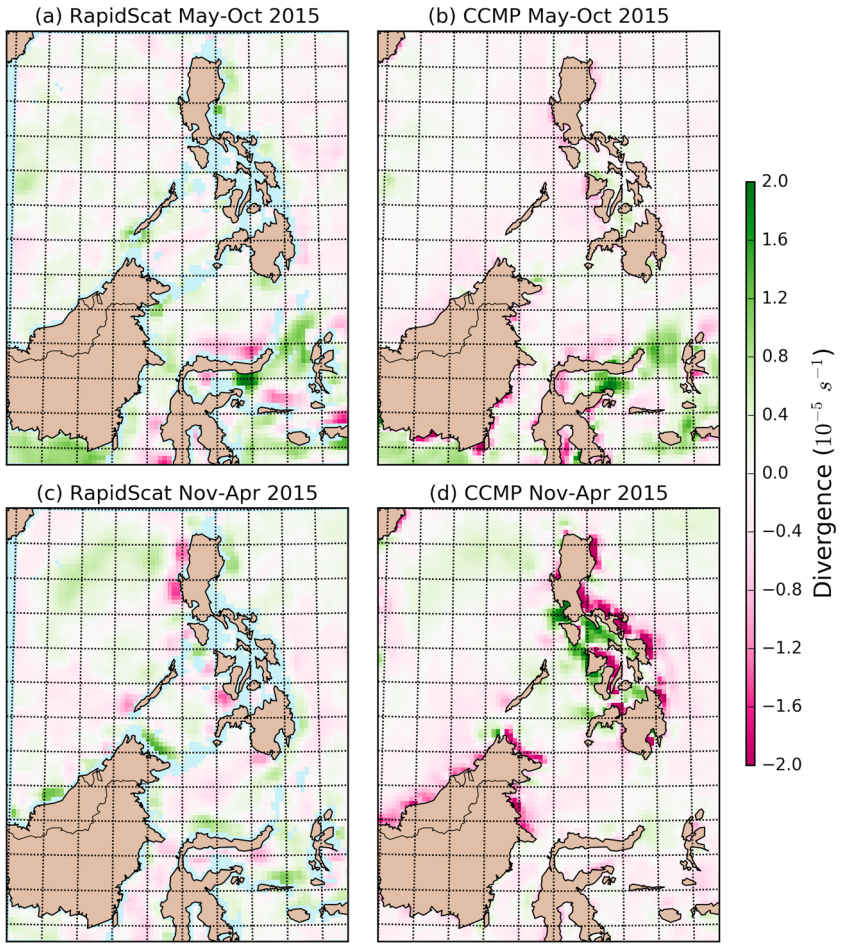

Figure 7. Seasonal means for divergence from RapidScat and CCMP. Gridlines are every 2°. (a) RapidScat May–October 2015. (b) CCMP May–October 2015. (c) RapidScat November–April 2015. (d) CCMP November–April 2015. RapidScat divergence has calculated on the swath, then binned and averaged, and finally smoothed using a 5 × 5 boxcar filter on the grid.

During the diurnal cycle, the winds rotate clockwise in agreement with the findings of Gille et al. (2016). The diurnal winds, both in terms of anomaly magnitude as well as $R^2 > 0.5$, impact the local flow up to ~200 km west of the island, suggesting that the island-driven wind effects have a long reach over the coastal ocean. However, this is a shorter distance than that of the diurnal impacts modeled by Park et al. (2011).

3.4. Divergence Comparison—CCMP Versus RapidScat

Figure 7 shows mean divergence comparisons between CCMP and RapidScat, for May–October 2015 (Figures 7a and 7b) and November–April 2015 (Figures 7c and 7d). A 5 × 5 boxcar smoothing operator has been applied to the RapidScat grid in order to clarify overall divergence patterns. Given the differences in how the divergence calculations were made between the two data sets (cf. section 2), the focus of the comparison will be on broad patterns rather than specific numbers.

In May–October (Figure 7b), CCMP indicates light convergence (typically $> -1 \times 10^{-5}$ s^{-1}) over much of the South China and Philippine Seas. RapidScat (Figure 7a) also suggests overall light convergence in these regions, but the pattern is more spatially variable, with isolated regions of light divergence mixed in. The two data sets disagree about the sign of the divergence off the northern coast of Borneo, with CCMP showing net convergence while RapidScat is more variable. There is some agreement near Sulawesi, especially with net convergence off the northern coast, as well as net divergence extending from east of the Gulf of Tomini toward the gap between North Sulawesi and Halmahera islands.

Table 1
Whole-Domain Differences in Divergence Between RapidScat and CCMP (i.e., RapidScat Minus CCMP) During 2015

	Bin and average		ZL1995-swath		ZL1995-grid		Rain flag removed	
	May–Oct	Apr–Nov	May–Oct	Apr–Nov	May–Oct	Apr–Nov	May–Oct	Apr–Nov
Mean (10^{-6} s^{-1})	1.24	1.03	0.88	0.59	0.42	0.59	1.23	0.99
Standard deviation (10^{-6} s^{-1})	3.67	3.93	3.81	4.30	3.62	4.04	3.53	3.74

Note. ZL1995 refers to *Zeng and Levy* (1995). Bin and average and Rain flag removed have had their RapidScat data smoothed by a 5 × 5 boxcar filter on the grid, prior to analysis.

During November–April 2015 (Figures 7c and 7d), the strong trade winds lead to net divergent flow in both data sets near the northwestern portion of the domain. However, there were notable areas of disagreement near the Philippines. On the windward (eastern) side strong convergence in CCMP was associated with braking of the flow by the terrain. RapidScat could not reproduce this. Divergence patterns on the leeward (westward) side were better matched, although significant disagreement in magnitudes remained. For example, immediately west of Luzon RapidScat observed two maxima in convergence. While CCMP also showed convergence in this region, it was much weaker. Alternatively, CCMP has stronger divergence than RapidScat near the Verde Island Passage, between Luzon and Mindoro. Significant disagreement between both data sets exists in magnitude and sign of divergence near Borneo. Agreement is better near Sulawesi, but not as good as May–October.

The effects of different approaches to divergence were also explored. Table 1 shows the domain average differences in divergence during 2015, excluding grid boxes with less than 400 RapidScat samples. As seen in Figure 7, over the open ocean there appeared to be a tendency toward more divergent flow in RapidScat, and this is confirmed by the domain statistics, with an offset on the order of 10^{-6} s^{-1}, depending on season. This offset is reduced if the Zeng and Levy (1995) interpolation approach is applied to the

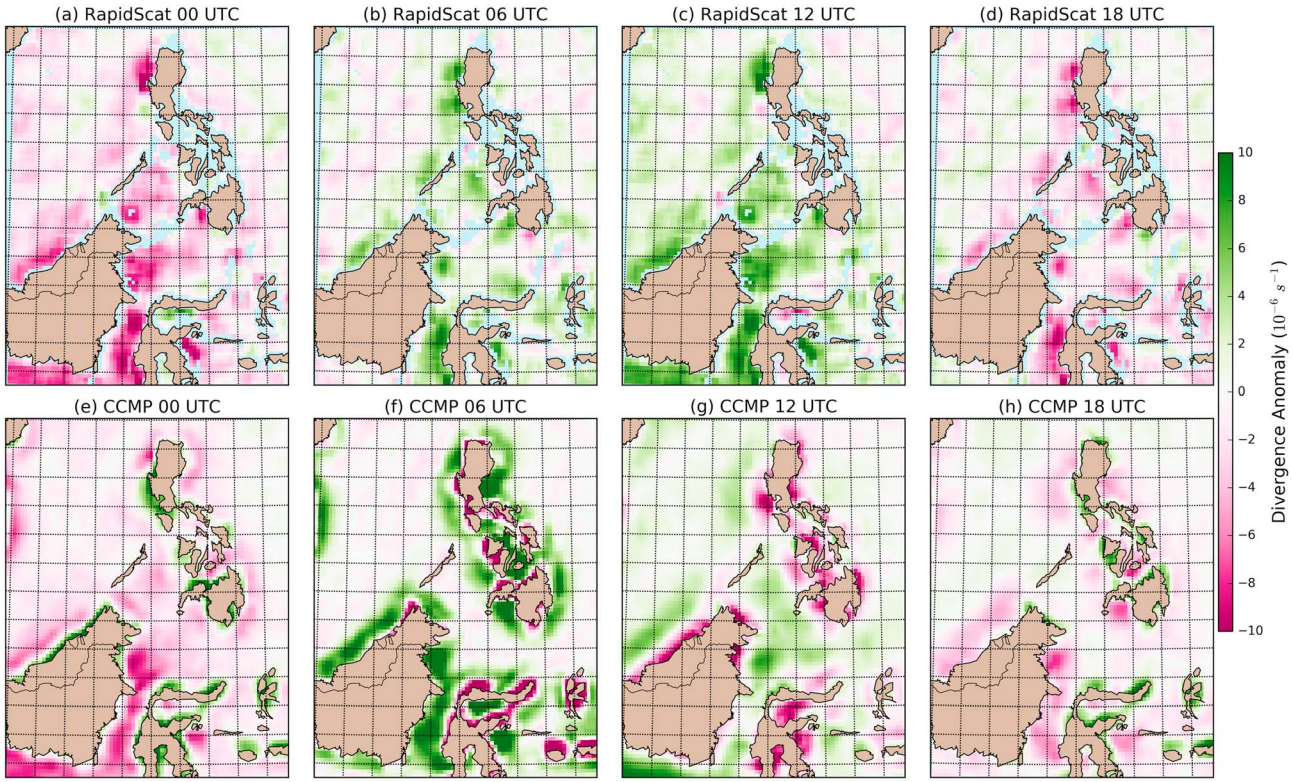

Figure 8. Divergence anomalies relative to the 3 October 2014 through 30 May 2016 RapidScat diurnal harmonic mean and CCMP mean, broken down by 6 h portions of the diurnal cycle. Gridlines are every 2°. (a) RapidScat at 0 UTC. (b) RapidScat at 6 UTC. (c) RapidScat at 12 UTC. (d) RapidScat at 18 UTC. (e) CCMP at 0 UTC. (f) CCMP at 6 UTC. (g) CCMP at 12 UTC. (h) CCMP at 18 UTC. RapidScat divergence anomaly has been smoothed using a 5 × 5 boxcar filter on the grid.

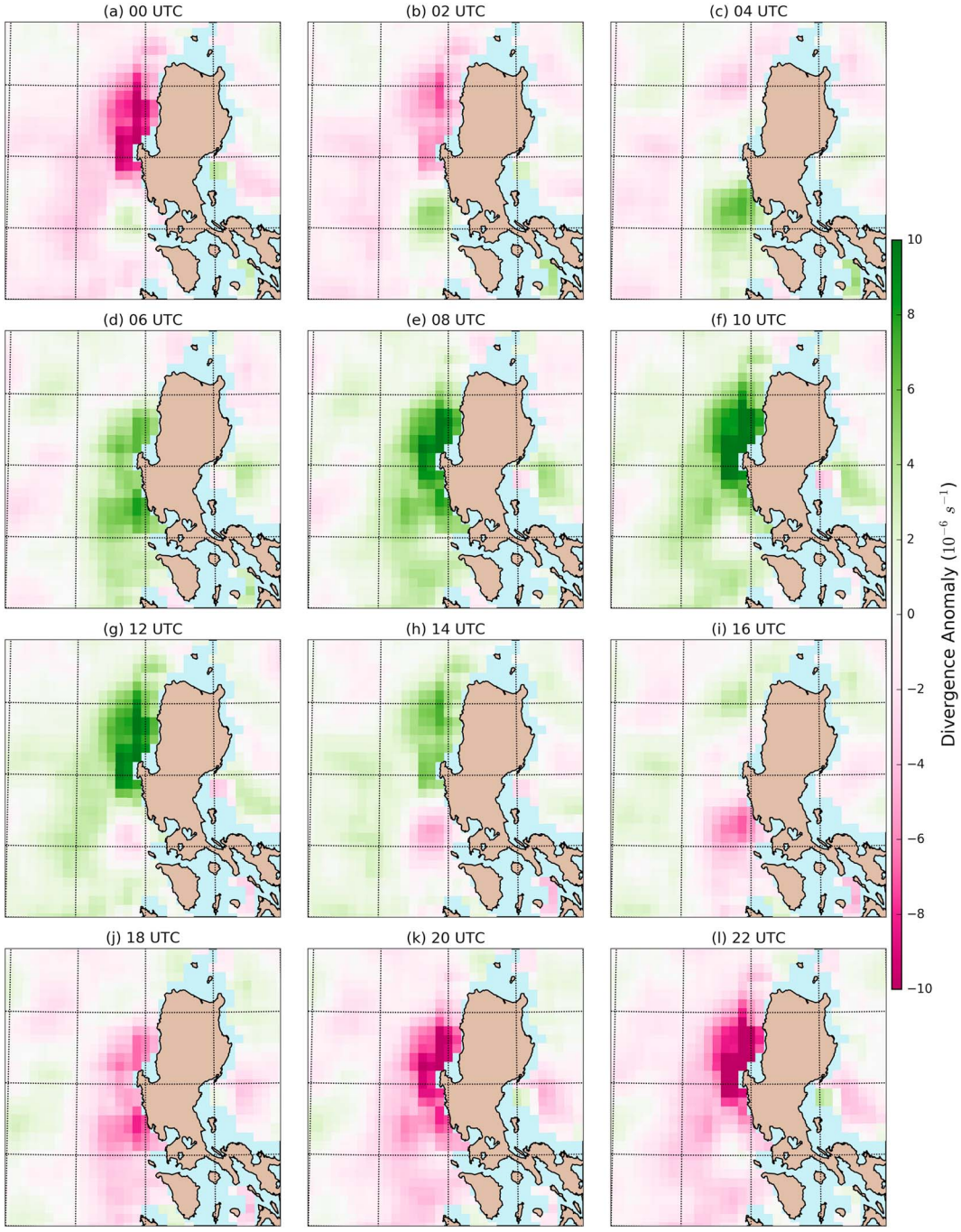

Figure 9. Divergence anomalies relative to the harmonic average for the entire RapidScat data set, broken down by 2 h portions of the diurnal cycle. Gridlines are every 2°. RapidScat divergence anomaly has been smoothed using a 5 × 5 boxcar filter on the grid.

swath-calculated divergence instead, although standard deviations are increased. The best overall agreement is achieved if the Zeng and Levy (1995) gridded RapidScat winds are used for the divergence calculations (i.e., Averages First, Derivatives Second or AFDS; O'Neill et al., 2015). This is unsurprising, since effectively the AFDS method is also what has been applied to CCMP, thereby reducing uncertainty due to differences in divergence techniques (the AFDS divergence maps are shown in Figure S6). Finally, only modest improvements with the bin-and-average technique are achieved if rain-flagged data are removed. This result is consistent with Milliff et al. (2004) in that—within the tropics at least—accounting for rain-flagged data may alter specific values for average vector wind derivatives but does not change

fundamental spatial patterns. Nevertheless, regardless of technique, there remains a more divergent tendency in the RapidScat data set for this domain.

The diurnal cycle of divergence was explored by comparing divergence anomalies relative to the means throughout the day, for the October 2014 through May 2016 period. For RapidScat, again to clarify spatial patterns, diurnal harmonics were fit to the 2-hourly binned-and-averaged data set before this differencing occurred. Results are shown in Figure 8. CCMP reveals alternatingly anomalously divergent and convergent "wave fronts" moving off significant land masses, such as Borneo and the Philippine archipelago, throughout the day. While RapidScat often matched the sign and even the strength of these divergence anomalies, particularly when examining areas beyond 100 km from coastlines, there are no indications of alternating "wave fronts" in that data set.

Near Luzon, there are significant differences in both the phasing and strength of the divergence diurnal cycle. RapidScat suggests the peak in the divergent anomaly off the west coast of the island occurs near 12 UTC, while CCMP places this closer at 6 UTC. Meanwhile, RapidScat sees much stronger convergent anomalies at 18 and 0 UTC. In order to explore this in more detail, the 2-hourly RapidScat results near Luzon are shown in Figure 9. Expectedly, the divergence anomalies match the wind harmonic anomalies shown in Figure 6. The morning offshore flow anomaly peak (22 and 0 UTC) is associated with enhanced convergence as the flow anomaly slows down far from shore. Meanwhile, the opposite occurs during the onshore peak near 10–12 UTC.

4. Discussion

The RapidScat and CCMP data sets agree broadly on the seasonal mean flows in most of this region. For example, both data sets capture the dramatic wind reversals associated with the monsoon, and the implications of these changes for the windward and lee sides of the Philippine archipelago. Notably, both data sets identify west of Luzon as an area of weak mean flow regardless of season.

This mean flow hides important diurnal variability, however. Alternating onshore and offshore flow patterns affect the winds up to approximately 200 km from the coast. According to RapidScat, the offshore flow is strongest in the morning hours (~0 UTC or 8 Local), and onshore flow is strongest in the early evening (~12 UTC or 20 Local). There is clockwise rotation of the wind anomalies between these two peaks. CCMP sees onshore flow being relative stronger at 6 UTC (14 Local) and relatively weaker at 12 UTC. The reasons for this are not clear, but the mean diurnal differences between RapidScat and CCMP are less than 0.4 m s^{-1} for either wind component (Figure 6), so it is not a large difference and may be within measurement uncertainty. Moreover, this small discrepancy is not an artifact of the diurnal harmonic, as simple averages of the RapidScat data throughout the diurnal cycle also suggest an onshore maximum near 10–12 UTC (not shown). This makes sense since the harmonic explained most of the diurnal wind variance west of Luzon.

One hypothesis is that flow channeling within the Lingayen Gulf contributes to this later maximum, because the onshore flow is more parallel to the Gulf opening at 10–12 UTC and wind speed anomalies are maximized near the mouth of the Gulf (Figure 6). RapidScat would be able to observe such a real effect, while the 0.25° resolution for the model producing the CCMP data set may not resolve the landmass gap well enough. Note, for example, how CCMP cannot reproduce the RapidScat-observed cyclonic curvature of May–October winds in the narrow Gulf of Tomini near Sulawesi, Indonesia (Figure 2). This would also explain why RapidScat sees relatively stronger offshore flow near 0 UTC, when the winds are again aligned with the Gulf but in the opposite direction.

A higher-resolution scatterometer, which could probe the interior of the Lingayen Gulf and other fine-scale waterways, would assist with further testing of this hypothesis. Reprocessing the RapidScat data to provide better coverage near coasts may help as well. Synthetic aperture radar (SAR) has proven to be very useful for studying gap flows near the Philippines at very high resolution (Gierach et al., 2012) and could also assist with such an analysis, although sample size would be a concern.

There are timing, sign, and magnitude discrepancies in divergence between RapidScat and CCMP near the Philippines and other coastlines. The disagreements in divergence near coastlines likely arise from three causes. One is the limited sampling by RapidScat near coasts, one is the limited spatial resolution of the CCMP model, and one is the nature of the CCMP data set. The first two have been discussed previously. In terms of the third possibility, CCMP winds are reported everywhere but are attenuated toward 0 m s^{-1}

over significant landmasses, such as Borneo and Luzon (CCMP is an ocean vector wind data set only; Atlas et al., 2011). This effectively creates windward braking (and leeward acceleration) effects in significant flow regimes, such as wintertime trade winds. Therefore, divergence disagreements between CCMP and RapidScat within ~100 km of coasts need to be considered in this context, and better agreement between the divergence data sets over the open ocean is both expected and observed in, for example, Figure 7. Regardless, RapidScat does observe in the net slightly more divergent flow over the domain ($0.4–1.2 \times 10^{-6}$ s^{-1} positive offset, depending on methodology).

It is hypothesized that the alternating "wave fronts" in the diurnal divergence anomalies, seen in the CCMP diurnal cycle (Figure 8), are also an artifact of how the CCMP model treats sea breeze effects. Specifically, the model likely does not treat the influence of moist convection on near-surface winds accurately, since its focus is on assimilation of scatterometer, radiometer, and buoy winds to produce an ocean vector wind data set, rather than modeling convection (Atlas et al., 2011).

Indeed, the complex interplay between topography, convection, and winds remains poorly understood, and is the subject of active research. For example, while daytime onshore flow near Luzon is likely driven by the land heating up (particularly aided by enhanced orography; Xie et al., 2006) to become warmer than the nearby sea surface temperatures (SSTs)—that is, a sea breeze—the origin of the offshore flow is less certain. It could be due to the land surface becoming cooler than surrounding SSTs during the nighttime (i.e., a true land breeze). However, given that this is a moist tropical environment, such nocturnal cooling is often mitigated by atmospheric water vapor, and thus it is unclear that a true land breeze circulation would occur on a regular basis.

Another possibility is related to the prolific diurnal convection that often occurs in concert with these observed circulations (Park et al., 2011). For example, the onshore flow is typically coincident with a rainfall maximum over Luzon (particularly during the monsoon), while the offshore flow is coincident with convection moving away from land (Park et al., 2011). Such convection could trigger a westward moving gravity wave, which would carry the convective signal and its associated outflows offshore (Aves & Johnson, 2008; Mapes et al., 2003). This signal also could manifest as nocturnal offshore flow. The ambiguity between land breeze and convectively driven mechanisms to explain the nocturnal offshore flow could be resolved by detailed investigation of the diurnal cycles of air temperature, SST, wind, and precipitation both in heavily convective meteorological regimes, as well as in suppressed ones.

5. Conclusions

The seasonal and diurnal cycles of ocean vector winds in the vicinity of the South China Sea and the Philippines have been characterized and compared using the RapidScat and CCMP data sets. Broad agreement exists between these data sets in terms of seasonal flow patterns. However, the diurnal wind patterns do not agree in all parts of this region. In many locations within the South China Sea, including west of Luzon, there is some disagreement in the magnitude and timing of vector winds and near-surface wind divergence between RapidScat and CCMP, and there also can be disagreement in divergence sign. The reasons for this are likely related to measurement uncertainty, as well as shortcomings in both the RapidScat (e.g., short data set length, lack of coastal coverage) and CCMP data sets (e.g., coarse temporal resolution, simplistic model characterization of winds near shore). These issues speak toward the urgent need for improved observations of seasonal, subseasonal, and diurnal wind variability within the South China Sea domain.

However, the analysis showed that RapidScat provided useful data for quantitatively characterizing the diurnal cycle of winds in otherwise poorly sampled regions like the South China Sea. This is because coverage was stable throughout the day, driving standard errors for wind components consistently below 0.5 m s^{-1} in most areas and times. Moreover, CCMP and RapidScat agreed well on directionality of the wind diurnal cycles, and the magnitudes of the wind component anomalies agreed within ±0.4 m s^{-1}. This implies that CCMP will be of value for examining, for example, intraseasonal variability of the diurnal cycle, particularly in a qualitative sense, since it is a much longer data set than RapidScat. Caution should be taken when examining CCMP divergence diurnal cycle, however, particularly near land. Finally, the analysis showed that the diurnal cycle near Luzon impacted winds up to ~200 km from shore and that topographic features may slightly amplify this effect due to flow channeling.

Acknowledgments
This research greatly benefitted from helpful discussions with the following people: Steve Rutledge, Weixin Xu, Steve Nesbitt, Georgios Priftis, Piyush Garg, Stella Choi, Themis Chronis, Greg King, and Mark Bourassa. Thank you to the anonymous reviewers who contributed to manuscript improvements. Funding for this work was provided by the NASA Ocean Vector Winds Science Team under the direction of Eric Lindstrom and from the Office of Naval Research PISTON project under the direction of Dan Eleuterio. CCMP Version 2.0 vector wind analyses are produced by Remote Sensing Systems, and the data are available at www.remss.com. RapidScat data are available from the NASA Physical Oceanography Distributed Active Archive Center (PO.DAAC). Analysis scripts may be obtained from the author (timothy.j.lang@nasa.gov). The views, opinions, and findings in this report are those of the author and should not be construed as an official NASA or U.S. Government position, policy, or decision.

References

Atlas, R., Hoffman, R. N., Ardizzone, J., Leidner, S. M., Jusem, J. C., Smith, D. K., & Gombos, D. (2011). A cross-calibrated, multiplatform ocean surface wind velocity product for meteorological and oceanographic applications. *Bulletin of the American Meteorological Society*, *92*, 157–174. https://doi.org/10.1175/2010BAMS2946.1

Aves, S., & Johnson, R. H. (2008). The diurnal cycle of convection over the northern South China Sea. *Journal of the Meteorological Society of Japan. Series II*, *86*(6), 919–934.

Birch, C. E., Webster, S., Peatman, S. C., Parker, D. J., Matthews, A. J., Li, Y., & Hassim, M. E. (2016). Scale interactions between the MJO and the Maritime Continent. *Journal of Climate*, *29*, 2471–2492.

Chan, J., Shi, J., & Lam, C. (1998). Seasonal forecasting of tropical cyclone activity over the western North Pacific and the South China Sea. *Weather and Forecasting*, *13*, 997–1004. https://doi.org/10.1175/1520-0434(1998)013<0997:SFOTCA>2.0.CO;2

Chen, T., & Chen, J. (1995). An observational study of the South China Sea monsoon during the 1979 summer: Onset and life cycle. *Monthly Weather Review*, *123*, 2295–2318. https://doi.org/10.1175/1520-0493(1995)123<2295:AOSOTS>2.0.CO;2

Chen, T., Tsay, J., Matsumoto, J., & Alpert, J. (2015). Development and formation mechanism of the Southeast Asian winter heavy rainfall events around the South China Sea. Part I: Formation and propagation of cold surge vortex. *Journal of Climate*, *28*, 1417–1443. https://doi.org/10.1175/JCLI-D-14-00170.1

Ciesielski, P., & Johnson, R. (2006). Contrasting characteristics of convection over the northern and southern South China Sea during SCSMEX. *Monthly Weather Review*, *134*, 1041–1062. https://doi.org/10.1175/MWR3113.1

Fang, G., Chen, H., Wei, Z., Wang, Y., Wang, X., & Li, C. (2006). Trends and interannual variability of the South China Sea surface winds, surface height, and surface temperature in the recent decade. *Journal of Geophysical Research*, *111*, C11S16. https://doi.org/10.1029/2005JC003276

Fore, A. G., Stiles, B. W., Chau, A. H., Williams, B. A., Dunbar, R. S., & Rodriguez, E. (2013). Point-wise wind retrieval and ambiguity removal improvements for the QuikSCAT Climatological Data Set. *IEEE Transactions on Geoscience and Remote Sensing*, *52*, 51–59. https://doi.org/10.1109/TGRS.2012.2235843

Fu, X., & Wang, B. (2004). Differences of boreal summer intraseasonal oscillations simulated in an atmosphere–ocean coupled model and an atmosphere-only model. *Journal of Climate*, *17*, 1263–1271.

Fukutomi, Y., & Yasunari, T. (2002). Tropical-extratropical interaction associated with the 10–25-day oscillation over the western Pacific during the northern summer. *Journal of the Meteorological Society of Japan*, *80*(2), 311–331.

Gierach, M. M., Graber, H. C., & Caruso, M. J. (2012). SAR-derived gap jet characteristics in the lee of the Philippine archipelago. *Remote Sensing of Environment*, *117*, 289–300. https://doi.org/10.1016/j.rse.2011.10.004

Gille, S. T., Llewellyn Smith, S. G., & Statom, N. M. (2005). Global observations of the land breeze. *Geophysical Research Letters*, *32*, L05605. https://doi.org/10.1029/2004GL022139

Gille, S., Nguyen, S., Northcott, D., Nutt, J., & Subramanian, A. (2016). Diurnal wind variability from RapidScat, International Ocean Vector Winds Science Team Meeting, Sapporo, Japan. https://mdc.coaps.fsu.edu/scatterometry/meeting/docs/2015/NewProductsAndApplications/gille_ovwst15.pdf

Hasager, C. B., Astrup, P., Zhu, R., Chang, R., Badger, M., & Hahmann, A. N. (2016). Quarter-century offshore winds from SSM/I and WRF in the North Sea and South China Sea. *Remote Sensing*, *8*, 769. https://doi.org/10.3390/rs8090769

Havens, G., & Poulson, L. (2016). RapidScat update, International Ocean Vector Winds Science Team meeting, Sapporo, Japan. https://mdc.coaps.fsu.edu/scatterometry/meeting/past.php#2016

Hayton, B. (2015). *The South China Sea: The Struggle for Power in Asia* (320 pp.). New Haven, CT: Yale University Press.

Hilburn, K. A., Meissner, T., Wentz, F. J., & Brown, S. T. (2016). Ocean vector winds from WindSat two-look polarimetric radiances. *IEEE Transactions on Geoscience and Remote Sensing*, *54*(2), 918–931. https://doi.org/10.1109/TGRS.2015.2469633

Ho, C.-H., Park, M.-S., Choi, Y.-S., & Takayabu, Y. N. (2008). Relationship between intraseasonal oscillation and diurnal variation of summer rainfall over the South China Sea. *Geophysical Research Letters*, *35*, L03701. https://doi.org/10.1029/2007GL031962

Hou, A., Kakar, R., Neeck, S., Azarbarzin, A., Kummerow, C., Kojima, M., … Iguchi, T. (2014). The global precipitation measurement mission. *Bulletin of the American Meteorological Society*, *95*, 701–722. https://doi.org/10.1175/BAMS-D-13-00164.1

Huang, W.-R., Chan, J. C. L., & Wang, S.-Y. (2010). A planetary-scale land–sea breeze circulation in East Asia and the western North Pacific. *Quarterly Journal of the Royal Meteorological Society*, *136*, 1543–1553. https://doi.org/10.1002/qj.663

Ichikawa, H., & Yasunari, T. (2006). Time–space characteristics of diurnal rainfall over Borneo and surrounding oceans as observed by TRMM-PR. *Journal of Climate*, *19*, 1238–1260. https://doi.org/10.1175/JCLI3714.1

Kim, H. M., Kim, D., Vitart, F., Toma, V., Kug, J., & Webster, P. J. (2016). MJO propagation across the Maritime Continent in the ECMWF ensemble prediction system. *Journal of Climate*, *29*, 3973–3988. https://doi.org/10.1175/JCLI-D-15-0862.1

Lau, K., Ding, Y., Wang, J., Johnson, R., Keenan, T., Cifelli, R., … Lin, P. (2000). A report of the field operations and early results of the South China Sea Monsoon Experiment (SCSMEX). *Bulletin of the American Meteorological Society*, *81*, 1261–1270. https://doi.org/10.1175/1520-0477(2000)081<1261:AROTFO>2.3.CO;2

Lee, J. Y., Wang, B., Wheeler, M. C., Wheeler, M. C., Fu, X., Waliser, D. E., & Kang, I.-S. (2013). Real-time multivariate indices for the boreal summer intraseasonal oscillation over the Asian summer monsoon region. *Climate Dynamics*, *40*, 493. https://doi.org/10.1007/s00382-012-1544-4

Li, W., Luo, C., Wang, D., & Lei, T. (2010). Diurnal variations of precipitation over the South China Sea. *Meteorology and Atmospheric Physics*, *109*, 33. https://doi.org/10.1007/s00703-010-0094-8

Lin, W., Portabella, M., Stoffelen, A., & Verhoef, A. (2017). Toward an improved wind inversion algorithm for RapidScat. *IEEE Journal of Selected Topics in Applied Earth Observations and Remote Sensing*, *10*(5), 2156–2164. https://doi.org/10.1109/JSTARS.2016.2616889

Love, B. S., Matthews, A. J., & Lister, G. M. S. (2011). The diurnal cycle of precipitation over the Maritime Continent in a high-resolution atmospheric model. *Quarterly Journal of the Royal Meteorological Society*, *137*, 934–947.

Madsen, N. M., & Long, D. G. (2016). Calibration and validation of the RapidScat scatterometer using tropical rainforests. *IEEE Transactions on Geoscience and Remote Sensing*, *54*(5), 2846–2854. https://doi.org/10.1109/TGRS.2015.2506463

Mapes, B. E., Warner, T. T., & Xu, M. (2003). Diurnal patterns of rainfall in northwestern South America. Part III: Diurnal gravity waves and nocturnal convection offshore. *Monthly Weather Review*, *131*, 830–844.

McGregor, S., Sen Gupta, A., Dommenget, D., Lee, T., McPhaden, M. J., & Kessler, W. S. (2017). Factors influencing the skill of synthesized satellite wind products in the tropical Pacific. *Journal of Geophysical Research: Oceans*, *122*, 1072–1089. https://doi.org/10.1002/2016JC012340

Milliff, R. F., Morzel, J., Chelton, D. B., & Freilich, M. H. (2004). Wind stress curl and wind stress divergence biases from rain effects on QSCAT surface wind retrievals. *Journal of Atmospheric and Oceanic Technology*, *21*, 1216–1231. https://doi.org/10.1175/1520-0426(2004)021<1216:WSCAWS>2.0.CO;2

National Geographic Society (2014). *Atlas of the world 2014* (Tenth ed). (pp. 448). Washington, D.C.: National Geographic Society.
O'Neill, L., Haack, T., & Durland, T. (2015). Estimation of time-averaged surface divergence and vorticity from satellite ocean vector winds. *Journal of Climate*, *28*, 7596–7620. https://doi.org/10.1175/JCLI-D-15-0119.1
Paget, A. C., Long, D. G., & Madsen, N. M. (2016). RapidScat diurnal cycles over land. *IEEE Transactions on Geoscience and Remote Sensing*, *54*(6), 3336–3344. https://doi.org/10.1109/TGRS.2016.2515022
Park, M. S., Ho, C. H., Kim, J., & Elsberry, R. L. (2011). Diurnal circulations and their multi-scale interaction leading to rainfall over the South China Sea upstream of the Philippines during intraseasonal monsoon westerly wind bursts. *Climate Dynamics*, *37*, 1483–1499. https://doi.org/10.1007/s00382-010-0922-z
Patoux, J., & Levy, G. (2013). Space-time interpolation of satellite winds in the tropics. *Journal of Geophysical Research: Atmospheres*, *118*, 10,405–10,413. https://doi.org/10.1002/jgrd.50811
Propagation of Intraseasonal Tropical Oscillations (2017). Propagation of Intra-Seasonal Tropical Oscillations (PISTON) [Available online at http://onrpiston.colostate.edu/]
Ploshay, J., & Lau, N. (2010). Simulation of the diurnal cycle in tropical rainfall and circulation during boreal summer with a high-resolution GCM. *Monthly Weather Review*, *138*, 3434–3453. https://doi.org/10.1175/2010MWR3291.1
RapidScat Project (2016). RapidScat level 2B climate ocean wind vectors in 12.5 km footprints. Ver. 1.0. PO.DAAC, CA, USA. Dataset accessed 2016–08-31 at https://doi.org/10.5067/RSX12-L2C11.
Sharma, N., & D'Sa, E. (2008). Assessment and analysis of QuikSCAT vector wind products for the Gulf of Mexico: A long-term and hurricane analysis. *Sensors*, *8*(3), 1927–1949.
Tang, W., Liu, W. T., Stiles, B., & Fore, A. (2014). Detection of diurnal cycle of ocean surface wind from space-based observations. *International Journal of Remote Sensing*, *35*(14), 5328–5341.
United States Department of Defense (2015). *Pentagon Report: Asia-Pacific Maritime Security Strategy: Achieving U.S. National Security Objectives-South China Sea, Japan, Senkaku Islands, Paracel, PLAN Navy, China's Spratlys Outposts* (411 pp.). Progressive Management.
Vitart, F., & Molteni, F. (2010). Simulation of the Madden– Julian Oscillation and its teleconnections in the ECMWF forecast system. *Quarterly Journal of the Royal Meteorological Society*, *136*, 842–855. https://doi.org/10.1002/qj.623
Wang, B., Ho, L., Zhang, Y., & Lu, M. (2004). Definition of South China Sea monsoon onset and commencement of the East Asia summer monsoon. *Journal of Climate*, *17*, 699–710. https://doi.org/10.1175/1520-0442(2004)017<0699:DOSCSM>2.0.CO;2
Wang, G., Chen, D., & Su, J. (2008). Winter eddy genesis in the eastern South China Sea due to orographic wind jets. *Journal of Physical Oceanography*, *38*, 726–732. https://doi.org/10.1175/2007JPO3868.1
Wang, J., Ge, C., Yang, Z., Hyer, E. J., Reid, J. S., Chew, B.-N., … Zhang, M. (2013). Mesoscale modeling of smoke transport over the Southeast Asian Maritime Continent: Interplay of sea breeze, trade wind, typhoon, and topography. *Atmospheric Research*, *122*, 486–503. https://doi.org/10.1016/j.atmosres.2012.05.009
Wang, Z., Stoffelen, A., Zhao, C., Vogelzang, J., Verhoef, A., Verspeek, J., … Chen, G. (2017). An SST-dependent Ku-band geophysical model function for RapidScat. *Journal of Geophysical Research: Oceans*, *122*, 3461–3480. https://doi.org/10.1002/2016JC012619
Wentz, F. J., Scott, J., Hoffman, R., Leidner, M., Atlas, R., & Ardizzone, J. (2015). Remote sensing systems Cross-Calibrated Multi-Platform (CCMP) 6-hourly ocean vector wind analysis product on 0.25 deg grid, Version 2.0. Remote Sensing Systems, Santa Rosa, CA. Available online at www.remss.com/measurements/ccmp. [Accessed 31 August 2016].
Wood, R., Köhler, M., Bennartz, R., & O'Dell, C. (2009). The diurnal cycle of surface divergence over the global oceans. *Quarterly Journal of the Royal Meteorological Society*, *135*, 1484–1493. https://doi.org/10.1002/qj.451
Wu, G., & Zhang, Y. (1998). Tibetan Plateau forcing and the timing of the monsoon onset over South Asia and the South China Sea. *Monthly Weather Review*, *126*, 913–927. https://doi.org/10.1175/1520-0493(1998)126<0913:TPFATT>2.0.CO;2
Xie, S., Xu, H., Saji, N., Wang, Y., & Liu, W. (2006). Role of narrow mountains in large-scale organization of Asian monsoon convection. *Journal of Climate*, *19*, 3420–3429. https://doi.org/10.1175/JCLI3777.1
Xie, S.-P., Chang, C.-H., Xie, Q., & Wang, D. (2007). Intraseasonal variability in the summer South China Sea: Wind jet, cold filament, and recirculations. *Journal of Geophysical Research*, *112*, C10008. https://doi.org/10.1029/2007JC004238
Yang, L., Du, Y., Wang, D., Wang, C., & Wang, X. (2015). Impact of intraseasonal oscillation on the tropical cyclone track in the South China Sea. *Climate Dynamics*, *44*, 1505. https://doi.org/10.1007/s00382-014-2180-y
Zeng, L., & Levy, G. (1995). Space and time aliasing structure in monthly mean polar-orbiting satellite data. *Journal of Geophysical Research*, *100*(D3), 5133–5142. https://doi.org/10.1029/94JD03252
Zhang, C. (2005). Madden-Julian Oscillation. *Reviews of Geophysics*, *43*, RG2003. https://doi.org/10.1029/2004RG000158
Zheng, C., Pan, J., & Li, J. (2013). Assessing the China Sea wind energy and wave energy resources from 1988 to 2009. *Ocean Engineering*, *65*, 39–48. https://doi.org/10.1016/j.oceaneng.2013.03.006
Zheng, C., Zhuang, H., Li, X., & Li, X. Q. (2012). Wind energy and wave energy resources assessment in the East China Sea and South China Sea. *China Technological Sciences*, *55*, 163. https://doi.org/10.1007/s11431-011-4646-z
Zierden, D. F., Bourassa, M. A., & O'Brien, J. J. (2000). Cyclone surface pressure fields and frontogenesis from NASA Scatterometer (NSCAT) winds. *Journal of Geophysical Research*, *105*(C10), 23,967–23,981. https://doi.org/10.1029/2000JC900062